

## Coulomb barriers and adsorbate effects in scanning tunneling microscopy

R. Berthe\* and J. Halbritter†

*Institut für Angewandte Physik, Universität Giessen, 6300 Giessen, Federal Republic of Germany*

(Received 25 September 1990)

Even in ultrahigh vacuum most surfaces studied by scanning tunneling microscopy (STM) and especially the STM tip are coated by adsorbates containing localized states. These localized states adjacent to the tip exhibit very small effective capacitances. For these small capacitances the Coulomb charging energy  $e^2/2C$  of an electron is large compared with the thermal energy  $kT$  even at room temperature. As a result, a Coulomb barrier shows up as the reduced tunnel current increases  $I \propto V^2$  for  $eV < e^2/2C$ . Spectroscopic  $I(V)$  data were analyzed for Nb and Au samples at different temperatures and tip-sample distances for wet-etched W tips. The  $I(V)$  characteristics revealed a Coulomb barrier in the resonant tunnel channel. Direct tunneling, which decreases more rapidly with tunnel distance, does not show this Coulomb barrier. The resonant tunnel channel shows that the Coulomb barrier seems to be related to the adsorbate ( $H_2O?$ ) at the W-WO<sub>3</sub> tip dominating tunneling under these circumstances. This explains the often reduced barrier height or atomic resolution in STM measurements.

### I. INTRODUCTION

Refined lithographic and low-temperature techniques allow the fabrication of devices whose behavior is affected by the capacitive charging energy of a single electron.<sup>1-3</sup> In comparison to the early work<sup>4-8</sup> on granular films with large random arrays of low-capacitance tunnel junctions, the small junction devices permit the study of quantum-mechanical phenomena without complications arising from collective actions. On the other hand, rigorous quantum-mechanical approaches<sup>9-11</sup> have led to a better understanding of the behavior of small junctions in the limit of small capacitances as well as to the prediction of a variety of interesting phenomena related to the quantum mechanics of such mesoscopic systems. However, in scanning tunneling microscopy (STM) it is still not clear if the charging blockade occurs between plane and tip being empty or via localized states of adsorbates or oxides, as found for planar junctions.<sup>12</sup> There it was found that in the resonant tunnel channel a Coulomb barrier shows up.

We will show in the following that in the case of an STM the Coulomb barrier occurs in the resonant tunnel channel,<sup>11</sup> which in parallel plane approximation is given by

$$j_{RT}(d) \propto n_M n_L \exp(-\kappa d). \quad (1.1)$$

The direct tunnel channel decays much more rapidly with barrier width  $d$ ,

$$j_s(d) \propto n_M^2 \exp(-2\kappa d). \quad (1.2)$$

In these equations<sup>11</sup>  $n_L$  is the density of localized states,  $n_M$  the density of states at the metallic banks, and

$$\kappa = \sqrt{2m(E_C - E_F)/\hbar},$$

a mean decay constant for the wave function of a tunneling electron in the barrier. For a tip of small radius  $R_T < 5$  nm, like for localized states, the three-dimensional decay of the wave function  $1/r \exp(-\kappa r)$  (Ref. 11) into

the barrier  $\Phi = E_C - E_F$  is more appropriate than the decay away from the plane  $\exp(-\kappa r)$ . Resonant tunneling is largest, for wave function amplitudes from both electrodes being equal at the localized site. Thus states adjacent to the tip dominate resonant tunneling and most imaging in STM is done in the resonant tunnel channel via states adjacent to the tip.

The theoretical analysis of Averin and Likharev<sup>10</sup> indicates that the  $I(V)$  characteristic is modified by a Coulomb blockade at low voltages showing for  $kT \ll e^2/2C$  a reduced increase:

$$I(V) = 2CV^2/\pi eR, \quad V \ll \Delta V = e/C. \quad (1.3)$$

At higher voltages a linear asymptote

$$I(V) = (V - \Delta V/2)/R, \quad V \gg \Delta V \quad (1.4)$$

is reached with  $R$  as resistance and  $\Delta V$  the displacement from the origin. Above,  $C$  denotes an effective charging capacitance, which has to be distinguished from an overall tip-plate stray capacitance as determined by usual ac-bridge measurements.  $C$  originates in the tip-to-plate volume being described by  $d$  as tip-plate distance and  $S$  as an effective area. This yields

$$\frac{1}{C_S} = \frac{d}{\epsilon_r \epsilon_0 S} \quad (1.5)$$

for the tip-plate capacitance and

$$\frac{1}{C_T} = \frac{1}{\epsilon_r \epsilon_0} \frac{1}{2(1 + r_T/R_T)^2 (2r_T + r_T^2/R_T)} \quad (1.6)$$

for the capacitance of a localized state  $r_T$  in front of a sphere ("tip") of radius  $R_T$ . Direct tunneling  $j_s$  [Eq. (1.2)] is accompanied by the capacitance  $C_S$  [Eq. (1.5)] and a resistance in the parallel-plane approximation,

$$R_S = R_0 \exp(2\kappa d), \quad (1.7)$$

where  $R_0 \propto 1/S$  holds. Resonant tunneling  $j_{RT} \propto 1/R_{RT}$  [Eq. (1.1)] is accompanied by an effective capacitance

$$C_{RT} = \alpha C_S + 1(\beta/C_p + \gamma/C_T) \quad (1.8)$$

describing the fact that a charge at  $r_T$  induces a small charge at the plane ( $C_p$ ) and a large charge at the tip ( $C_T$ ), where the latter induces its counterpart ( $C_S$ ) at the plane. For example,  $\alpha=0$  and  $\beta=\gamma=0.5$  holds for parallel-plane geometry for states in the middle of the barrier.<sup>12</sup> For increasing asymmetry  $r_T/d \rightarrow 0 \approx 1 \approx \beta$  and  $\gamma \ll 1$  is predicted in Eq. (1.8).  $C_p$  given by

$$1/C_p = 1/[\epsilon_{rp}\epsilon_0 4(d-r_T)] \quad (1.9)$$

is the capacitance relative to the plane of the localized state at  $r_T$  in front of the tip. As an estimate for the tip-plane capacitance  $C_S$  we assume  $\sqrt{S} \approx 2 \text{ nm} \approx d$  yielding for  $\epsilon_r \approx 20$ ,

$$\frac{e^2}{C_S} = 0.112 \text{ eV} . \quad (1.10)$$

As indicated in Eq. (1.8) the charging energy in resonant tunneling is smaller than that given in simple parallel plates. But for states close to the tip, i.e., small  $r_T$ , the charging energy is high due to the large asymmetry  $\alpha \approx 1$ . These states carry most of the resonant tunnel current due to the equal amplitude from the tip ( $\propto \exp[-\kappa(R_T+r_T)]/(R_T+r_T)$ ) and plane ( $\propto \exp[-\kappa(d-r_T)]$ ) and thus their Coulomb barrier will show up. For comparison with experiments we make use of the dominant exponential dependencies of the tunnel currents on distances in Eq. (1.1), where the capacitance depends roughly like  $1/d$  on tip-plate distance. Thus, logarithmic plots of  $R_S$  or  $R = 1/(1/R_{RT} + 1/R_S)$  versus  $1/C$  are used in the following.

In this paper, we report local spectroscopic STM measurements on niobium and gold samples by electrochemically etched W-tips at various temperatures.<sup>13,14</sup>

## II. EXPERIMENT

The samples have been cut from polycrystalline foils. Large grains in the order of  $100 \mu\text{m}$  diameter were obtained by performing the usual ultrahigh vacuum annealing procedures. The details of the Nb-sample preparation are described in Ref. 13, where it is reported that Nb is coated by  $\text{Nb}_2\text{O}_5$  ( $\approx 2 \text{ nm}$ ) exhibiting an effective barrier height of  $\Phi \approx 0.1-0.9 \text{ eV}$ , and by an adsorption layer ( $-\text{OH}$ ,  $-\text{COH}$ , . . .) in excess of  $2 \text{ nm}$  thickness. These ten monolayers<sup>15</sup> have been found as equilibrium for  $\text{Nb}_2\text{O}_5$  (Ref. 13) after 1 day in  $10^{-9}$ -Torr UHV at  $300 \text{ K}$ . Dry  $\text{Nb}_2\text{O}_5$  or Au surfaces have about 2-to-4 monolayers of adsorbates under similar UHV conditions. The electrochemically etched W-tip is coated<sup>16</sup> by 1-3-nm amphoteric  $\text{WO}_3$  (W-OH) whereby OH groups  $\text{H}_2\text{O}$  or hydrocarbons are bonded like in the case of  $\text{Nb}_2\text{O}_5$ .<sup>13,15</sup> Thus, in our STM system ( $\approx 10^{-5}$  Torr vacuum or He exchange gas with a purity corresponding to about  $10^{-3}$  Torr),<sup>13</sup> in particular at lower temperature due to cryopumping, a much thicker adsorbate layer ( $> 5 \text{ nm}$ ) covers the sample and tip. Thus in STM measurements the tip necessarily steers in this adsorbate contamination.

The experimental setup consists of a compact STM

which was mounted in a helium cryostat. All measurements have been performed in a helium exchange gas atmosphere at normal pressure. Rough positioning of the tip was done from outside the cryostat with a differential screw mechanism. Fine positioning, i.e., variation of the tip-to-sample distance as well as of the actual lateral probe position, has been achieved in the usual manner using a piezotube scanner. The time constant of the STM feedback electronics could be adjusted in a way that thermal drift and low-frequency vibrations are compensated, while full  $I(V)$  characteristics ( $\approx \text{nA}$ ) are swept at a frequency of about  $1 \text{ kHz}$ .<sup>13</sup>

## III. RESULTS AND DISCUSSION

Figure 1 shows a typical result for the niobium sample at a temperature of  $300 \text{ K}$ . The low-voltage nonlinearity Eq. (1.3) of the  $I(V)$  curve is clearly seen in Fig. 1(a). At higher voltages the characteristic becomes linear and barrier-induced effects at  $\text{eV} \approx \Phi$  are not observed up to about  $0.9 \text{ eV}$ , i.e.,  $\Phi > 0.9 \text{ eV}$  holds. This linear dependence is made obvious in a plot of the dynamic conductance  $dI/dV$  in Fig. 1(b). At sufficiently high voltages [ $V > \Delta V$ , Eq. (1.4)] the dynamic conductance becomes constant and is dominated by the tunneling conductance  $1/R$  given by Eq. (1.4). An additional feature revealed by Figs. 1(b) and 1(c) is the existence of a shunt conductance  $1/R_s$  which corresponds to a finite initial slope of the  $I(V)$  characteristic in Fig. 1(a). It has been confirmed by static measurements that this shunt conductance is not an artifact of the measurements, e.g., resulting from phase-lag effects, but is a reproducible feature of the STM junctions. As discussed below and indicated by its temperature independence,  $R_s$  is related to direct tunneling [Eq. (1.2)]. In Figs. 1 and 2 the  $I(V)$  curve for the Nb sample at  $77$  and  $4.2 \text{ K}$  are shown. Using the asymptotes shown in Fig. 1(a), the charging capacitance  $C$  from Eq. (1.3), as well as the resistance  $R$ , can be determined. It is confirmed by Fig. 2 that the predicted low-voltage quadratic behavior coincides well with the experimentally recorded curve.

The  $I(V)$  characteristics shown in Figs. 1 and 2 reveal that at low voltages STM tunneling is hindered by a Coulomb barrier (or blockade). This Coulomb barrier seems to be a general effect occurring at widely different resistances, temperatures, and electrode materials for our W tips. Such a Coulomb barrier has also been found for a planar tunnel barrier<sup>12</sup> in the resonant tunnel channel. Thus we claim that resonant tunneling via localized states is the site for the Coulomb barrier, as in  $\text{Nb}_2\text{O}_5$  (Ref. 11) or a-Si.<sup>12</sup> In line with resonant tunneling is the scatter of  $R$  and  $C$  in Figs. 3-5 around the indicated mean value being related to statistical changes of the localized states carrying the tunnel current.

The above separation  $1/R = 1/R_{RT} + 1/R_S$  (Fig. 1) has even quantitatively all the properties of resonant and direct tunneling proposed in Eqs. (1.1) and (1.2). This is shown in Fig. 3 by  $R$  being much smaller than  $R_S$  so that the plot  $\log_{10} R \approx \log_{10} R_{RT} \propto \kappa d$  versus  $\log_{10} R_S \propto 2\kappa d$  has to yield a straight line with slope 0.5 as found in our experiments. This slope 0.5 is also showing up in the

work-function measurement  $dI/dd$  yielding with Eq. (1.2) 0.9 eV as barrier height  $\Phi$ .<sup>13</sup> At 0.9 eV the current does not show any increase proving this barrier height.<sup>11</sup> In contrast, the use of Eq. (1.1) yields  $\Phi \approx 3.6$  eV  $= 4 \times 0.9$  eV being in line with standard work functions. This shows that also in earlier STM measurements<sup>14</sup> resonant tunneling was the dominant tunnel channel.

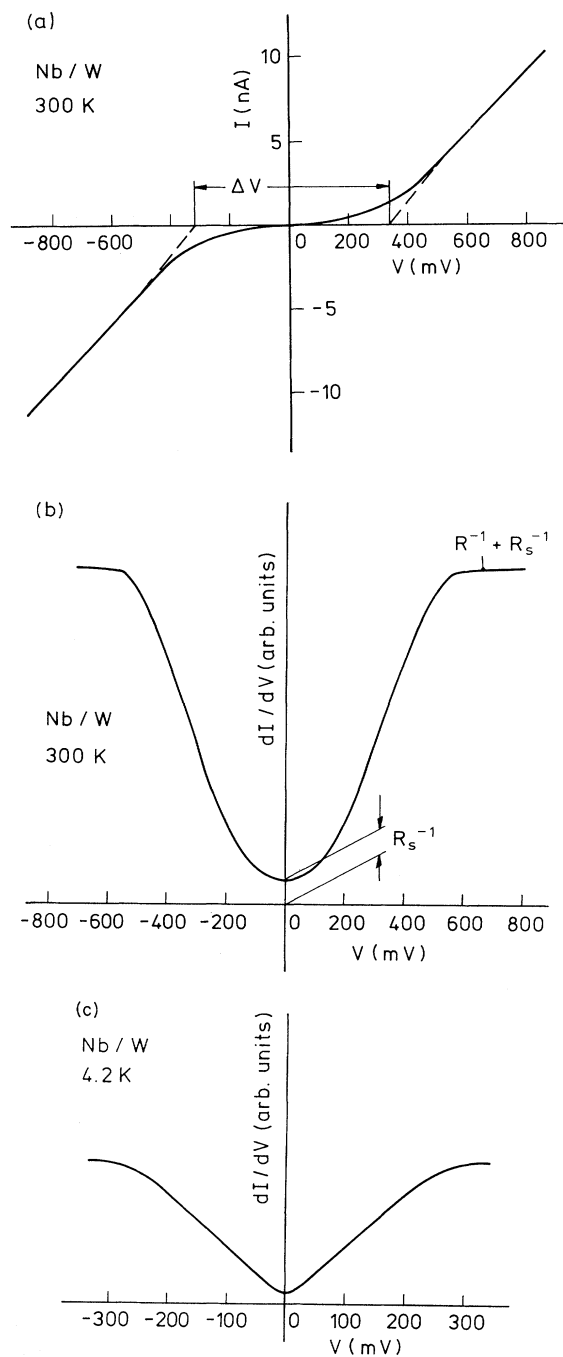


FIG. 1. (a)  $I(V)$  characteristic recorded with a tungsten tip on a niobium sample at 300 K. The parallel asymptotes are indicated for reference. (b) Corresponding dynamic conductance  $dI/dV$ . (c) Dynamic conductance for the same sample at 4.2 K.

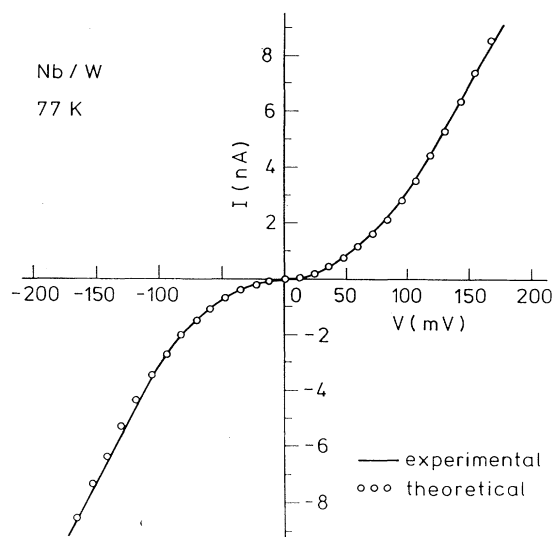


FIG. 2. Experimentally recorded  $I(V)$  curve (solid line) in comparison with theoretical points for the niobium sample at 77 K. The theoretical points are calculated without any adjustable parameters according to Eqs. (1.3) and (1.4) (Ref. 10).

Figure 3 shows that for Nb and Au samples and  $300\text{ K} \geq T \geq 4.2\text{ K}$  identical  $R_S$  are obtained despite widely differing  $R$  values. This confirms our point of view that  $R_S$  is describing direct tunneling and  $2\kappa d$  the barrier. Then Fig. 3 indicates for Nb that  $R_{RT}$  is much smaller than  $R_S$  and increases with  $T$ , in contrast to Au. Both observations are explained by  $\text{Nb}_2\text{O}_5$  coating Nb and containing low  $\Phi$  channels ( $< 1$  eV), which enhance  $1/R_{RT}$  locally and showing a conductance decreasing with increasing temperature.<sup>17</sup> In contrast Au adsorbates have a uniform barrier and a resonant tunnel conductance increasing with temperature which is explainable by inelastic tunneling.<sup>18</sup>

The question is now, where are the localized states coming from causing the observed resonant tunneling? In planar junctions resonant tunneling is dominated by states in the middle of the barrier because of equal amplitudes from both electrodes.<sup>11,12</sup> In contrast in STM, states adjacent to the narrow tip carry most of the resonant tunnel current as discussed above. The electrochemically etched W tip is coated by 1–3-nm  $\text{WO}_3\text{-W-OH}$  (Ref. 16) bonding  $\text{H}_2\text{O}$  and hydrocarbons. The shape resonances of these adsorbates are the most likely candidates for states carrying resonant tunneling as found in secondary electron emissions of  $\text{Nb}_2\text{O}_5\text{-NbOH}$ .<sup>15</sup>

For such states  $r_T$  adjacent to the tip Eq. (1.8) gives the appropriate Coulomb barrier, where  $\alpha$  and  $\beta$  approach 1 with asymmetry. The charging energy  $e^2/C_{RT}$  increases with  $d$  mainly by  $\alpha C_s \propto S/d$  with a small  $S < 2\text{ nm}^2$  because it is due to an adjacent image charge. This describes Figs. 4 and 5. For a quantitative discussion  $\log_{10} R_S$  versus  $1/C_{RT}$  for Nb-Nb<sub>2</sub>O<sub>5</sub>-adsorbate-WO<sub>3</sub>-W is plotted in Fig. 4 showing roughly the same linear  $\kappa d$  versus  $1/C_{RT}$  dependence for 4 and 77 K, only for 300 K,  $1/C_{RT}$  becomes larger. This  $1/C_{RT}$  increase from 4

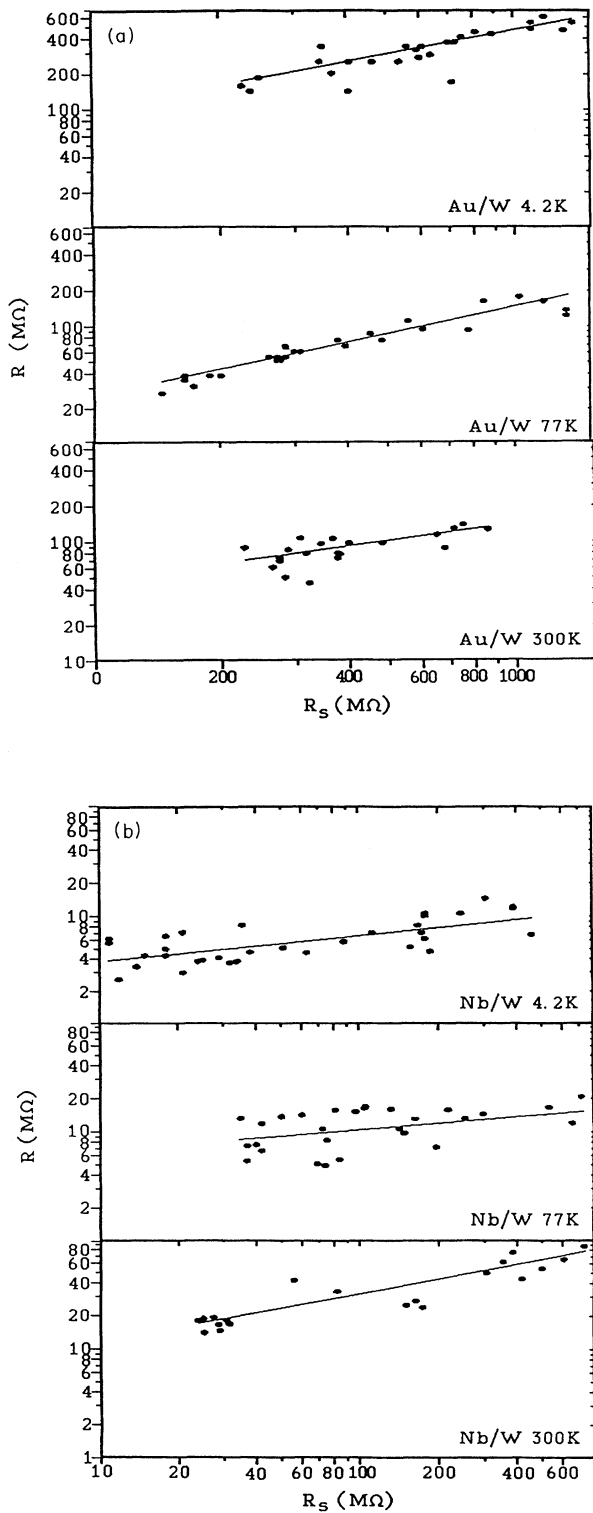


FIG. 3. Resistance  $R$  vs  $R_S$  showing that  $\log_{10}R$  increases with  $\log_{10}R_S$  roughly linearly with a slope 0.5. This confirms  $\log_{10}R \approx \log_{10}R_{RT} \propto \kappa d$  vs  $\log_{10}R_S \propto 2\kappa d$ . Remarkable is the fact that  $R_{RT}$  for Nb samples is smaller than for Au samples, but  $R_S$  is roughly independent of  $T$  and plane material. This proves that only direct tunneling  $R_S$  describes the plane-tip barrier.

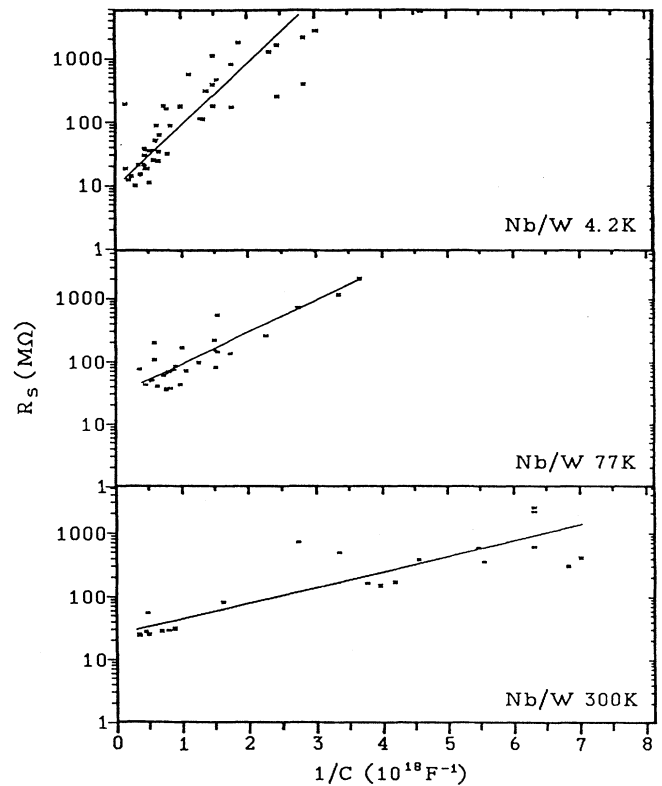


FIG. 4. The direct tunnel resistance  $R_S$  vs the inverse charging capacitance for Nb at 4.2, 77, and 300 K. The scatter of the data around the least-square fits can be related to different localized states with different charging energies and different tunnel geometries.

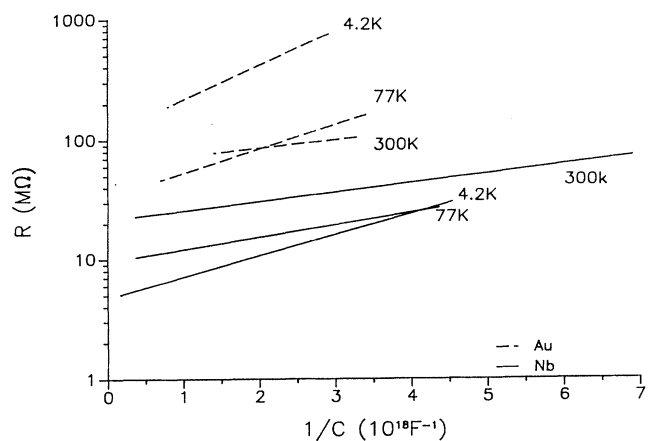


FIG. 5. The tunneling resistance vs the inverse capacitance for the niobium and gold sample at various temperatures. The lines are least-squares fits according to  $1/C \propto \log_{10}R$  to the experimentally obtained points. As shown in Fig. 3 the widely differing  $R$  values are related to differing resonant tunneling and thus do not reflect the plane-tip geometry.

to 300 K is likely a consequence of the reduced density of the adsorbates above 100 K causing an  $\epsilon_r$  reduction. Comparing Fig. 4 with Fig. 5 one realizes that  $\log_{10}R_s$  changes by 1 order of magnitude for roughly 1 order change of  $1/C_{RT}$ . In contrast in Fig. 5,  $\log_{10}R$  changes less than  $1/C_{RT}$  like in Refs. 1–3, confirming our point of view that only  $\log_{10}R_s \propto 2\kappa d$  is a measure of the tip sample barrier.

The above consistent picture relating most of imaging in STM to resonant tunneling via states adjacent to the tip is supported by the measurements of Kirk.<sup>19</sup> He showed in addition to resonant tunneling yielding a Coulomb barrier that organic molecules adjacent to the tip enhance the tunnel current and yield steps in  $dI/dV$ . These steps at excitation energies of the molecule prove the opening of a new tunnel channel, which cannot be explained by standard inelastic tunneling. We propose that these “inelastic resonant tunnel channels” are due to inelastic processes being determined by the shape resonance showing a large overlap with tip wave functions yielding resonant tunneling, as observed.<sup>19</sup>

#### IV. CONCLUSION

Our spectroscopic STM measurements provide clear evidence for correlated single electron tunneling up to room temperature. The general occurrence of the Coulomb blockade is not based on a peculiar density of

surface states, but rather is a fundamental physical phenomena of tunnel junctions with a sufficiently small inherent capacitance. The actual Coulomb charging of a single electron is related to resonant tunneling via localized states adjacent to the tip in the tunnel barrier. This fact sheds light on the tunnel time or capacitance discussions. In the present study—as is often the case in STM and atomic force microscope (AFM) measurements—the interelectrode spacing is filled by oxides, hydroxides, and adsorbates. Under the different states in the barrier electron attachment states bonded to the tip like W-OH-HOH, are the prominent cause for this resonant tunneling. This atomic tip sharpening by resonant tunneling may yield good scanning operation with atomic resolution, whereas the  $I(V)$  spectroscopic operation is disturbed by the Coulomb barrier. This was confirmed recently by dry Pt-Ir tips showing better  $I(V)$  results.<sup>13</sup> It is obvious that these adsorbates play a crucial role in the AFM and its irreversibilities, because the acoustic energy transferred from sample to cantilever via adsorbates (capillary forces) dominates over, e.g., van der Waals forces.

#### ACKNOWLEDGMENTS

Thanks are due to M. Anders for his continuous technical assistance in operating the STM and to W. Harrison, C. Heiden, and M. Kirk for many valuable discussions.

\*Present address: Kernforschungsanlage Jülich, Institut für Schicht und Ionentechnik, W-5170 Jülich, Germany.

†Present address: Kernforschungszentrum Karlsruhe, Institut für Material und Festkörperforschung I, W-7500 Karlsruhe, Germany.

<sup>1</sup>T. A. Fulton and G. J. Dolan, Phys. Rev. Lett. **59**, 109 (1987).

<sup>2</sup>M. Iansiti, A. T. Johnson, W. F. Smith, H. Rogalla, C. J. Lobb, and M. Tinkham, Phys. Rev. Lett. **59**, 489 (1987).

<sup>3</sup>P. J. M. van Bentum, H. van Kempen, L. E. C. van de Leemput, and P. A. A. Teunissen, Phys. Rev. Lett. **60**, 369 (1988).

<sup>4</sup>I. Giaever and H. R. Zeller, Phys. Rev. Lett. **20**, 1505 (1968).

<sup>5</sup>J. Lambe and R. C. Jaklevic, Phys. Rev. Lett. **22**, 1371 (1969).

<sup>6</sup>R. Cavicchi and R. H. Silsbee, Phys. Rev. Lett. **52**, 1453 (1985).

<sup>7</sup>B. G. Orr, H. M. Jaeger, A. M. Goldman, and C. G. Kuper, Phys. Rev. Lett. **56**, 378 (1986).

<sup>8</sup>E. Ben Jacob and Y. Gefen, Phys. Rev. Lett. **108A**, 289 (1985).

<sup>9</sup>A. I. Larkin, K. K. Likharev, and Y. N. Ovchinnikov, Physica **126B+C**, 414 (1984).

<sup>10</sup>D. V. Averin and K. K. Likharev, J. Low Temp. Phys. **62**, 345 (1986).

<sup>11</sup>J. Halbritter, Surf. Sci. **122**, 80 (1982); **159**, 509 (1985).

<sup>12</sup>M. Naito and M. R. Beasley, Phys. Rev. B **35**, 2548 (1987).

<sup>13</sup>R. Berthe, Dr. rer. nat. thesis, Universität Giessen, Germany, 1991.

<sup>14</sup>G. Binnig, R. Rohrer, Ch. Gerber, and E. Weibel, Phys. Rev. Lett. **49**, 57 (1982); **50**, 120 (1984).

<sup>15</sup>M. Grundner and J. Halbritter, J. Appl. Phys. **51**, 5396 (1980); J. Halbritter, IEEE Trans. **EI-20**, 671 (1985), and references therein.

<sup>16</sup>W. Lisowski, G. Kip, A. H. J. van der Berg, and L. I. Hanskamp, Fresenius' Z Anal. Chem. (to be published).

<sup>17</sup>J. Halbritter, Appl. Phys. A **43**, 1 (1987), and references therein.

<sup>18</sup>Y. Xu, A. Matsuda, and M. R. Beasley, Phys. Rev. B **42**, 1492 (1990).

<sup>19</sup>M. D. Kirk, Ph.D. thesis, Stanford University, 1989.